PHOTONICS Research

Q-switched and mode-locked Er-doped fiber laser using $PtSe_2$ as a saturable absorber

Kang Zhang,[1] Ming Feng,[1,*] Yangyang Ren,[1] Fang Liu,[1] Xingshuo Chen,[1] Jie Yang,[1] Xiao-Qing Yan,[1,2] Feng Song,[1] and Jianguo Tian[1]

[1]Key Laboratory of Weak-Light Nonlinear Photonics, Ministry of Education, School of Physics and TEDA Applied Physics School, Nankai University, Tianjin 300071, China
[2]e-mail: yanxq01@nankai.edu.cn
*Corresponding author: mingfeng@nankai.edu.cn

Received 14 June 2018; revised 25 July 2018; accepted 25 July 2018; posted 25 July 2018 (Doc. ID 335211); published 23 August 2018

We report a passively *Q*-switched and mode-locked erbium-doped fiber laser (EDFL) based on $PtSe_2$, a new two-dimensional material, as a saturable absorber (SA). Self-started *Q*-switching at 1560 nm in the EDFL was achieved at a threshold pump power of 65 mW, and at the maximum pump power of 450 mW, the maximum single *Q*-switched pulse energy is 143.2 nJ. Due to the polarization-dependent characteristics of the $PtSe_2$-based SA, the laser can be switched from the *Q*-switched state to the mode-locked state by adjusting the polarization state. A mode-locked pulse train with a repetition rate of 23.3 MHz and a pulse width of 1.02 ps can be generated when the pump power increases to about 80 mW, and the stable mode-locked state is maintained until the pump power reaches its maximum 450 mW. The maximum single mode-locked pulse energy is 0.53 nJ. This is the first time to our knowledge that successful generation of stable *Q*-switched and mode-locked pulses in an Er-doped fiber laser has been obtained by using $PtSe_2$ as a saturable absorber.

OCIS codes: (140.3510) Lasers, fiber; (140.7090) Ultrafast lasers; (140.3380) Laser materials; (160.4670) Optical materials.

https://doi.org/10.1364/PRJ.6.000893

1. INTRODUCTION

Q-switching and mode-locking are two main ways to generate pulses [1–4]. Among the two technologies, saturable absorbers (SAs) play a vital role in passive *Q*-switching and mode-locking [5–13]. Fiber lasers have the advantages of simple structure, small size, low price, and high environmental stability [12–17]. Therefore, it is clear that the development of pulsed lasers depends greatly on the development of saturable absorbing materials. Traditional SAs, such as semiconductor saturable absorber mirrors (SESAM), face many defects, such as narrow working bandwidth and complex manufacturing packages, which greatly limit the development of pulsed lasers. With the advancement of material science, new nanomaterials such as carbon nanotubes (CNTs) [8,9], graphene [10–12], graphene oxide [13], black phosphorus (BP) [17,18], and topological insulators (TI) [19–22] have emerged one after another, and their performance has been qualitatively improved as their prices have declined. Recently, transition-metal dichalcogenides (TMDs) (e.g., MoS_2 [23], WS_2 [24,25], TiS_2 [26], $MoTe_2$ [27,28]) have attracted much attention from laser researchers due to their thickness-dependent band gap and unique absorption property [29,30]. $PtSe_2$ also attracts our attention as a new member of the layered TMDs family [31–35]. $PtSe_2$'s characteristic of having a widely tunable band gap allows it to effectively respond to near-infrared light, and its photoresponsivity is comparable with that of BP [36]. Monolayer $PtSe_2$ has an indirect band gap of about 1.2 eV, while the band gap of double-layered $PtSe_2$ is reduced to 0.21 eV. Three or more layers of $PtSe_2$ have a zero band gap, and the macroscopic properties are represented by semimetals [31]. Compared to MoS_2, a TMD material that has been widely studied in the field of laser mode-locking, $PtSe_2$ has a higher carrier mobility that is comparable to that of graphene [35–38]. Therefore, it can produce a fast nonlinear response to incident light and can achieve narrower pulses. In addition, the narrower energy band gap of $PtSe_2$ allows it to have nonlinear effects in a wider wavelength range. Moreover, the characteristics of the zero bandgap of multi-layered $PtSe_2$ and the high carrier mobility are similar to graphene, although there is a large difference in the band structures. Therefore, $PtSe_2$ has the potential to substitute for graphene as an excellent SA.

In this paper, we report an erbium-doped fiber laser (EDFL) based on $PtSe_2$ as an SA with obvious polarization-dependent saturable absorption, and we have obtained both passive *Q*-switching and mode-locking pulses. As far as we know,

it is the first time that $PtSe_2$ has been used as an SA for both *Q*-switching and mode-locking in a fiber laser.

2. EXPERIMENTAL SETUP

In our experiment, the $PtSe_2$ thin films are grown by the chemical-vapor-deposition (CVD) technology on a sapphire substrate, which are commercial products (6 Carbon Technology, Shenzhen, China). The optical microscope image shows that the grown $PtSe_2$ film exhibits a good continuous uniformity over a large area (not shown here). The surface morphology and height profile of the $PtSe_2$ thin film are obtained from atomic force microscopy (AFM) imaging, as shown in Fig. 1(a). From the AFM image, the thickness of the used $PtSe_2$ film is determined to be 4.7 ± 0.4 nm by the height profile, indicating that the number of layers of the $PtSe_2$ sample is around five. The Raman spectrum of the $PtSe_2$ film is shown in Fig. 1(b). Three characteristic peaks could be observed: (1) the peak at 179.6 cm^{-1}, corresponding to the in-plane vibration of Se atoms in opposite directions within a single layer, (2) the peak at 206.5 cm^{-1}, which corresponds to out-of-plane vibration of Se atoms, (3) and the longitudinal optical (LO) peak at 235.4 cm^{-1}, which is attributed to the overlap of the A2u mode and Eu mode. The Raman spectrum observed here is in good agreement with that reported in Ref. [39]. The linear absorption of the $PtSe_2$ film was measured in the range from 200 to 1600 nm using a Hitachi spectrophotometer, and broadband absorption can be observed in Fig. 1(c). The absorption peak characterized by a flat profile is located between 409 and 652 nm, and 1600 nm is at the absorption edge, showing that the used $PtSe_2$ films have the potential of working as SAs in the near-infrared region. Measurements on different positions yield nearly identical results, confirming the uniformity of the $PtSe_2$ films.

The $PtSe_2$-based SA is fabricated with a $PtSe_2$-covered-microfiber structure, as shown in Fig. 2(a). First, we transfer the $PtSe_2$ film from the sapphire substrate onto a polydimethylsiloxane (PDMS) sheet. To avoid the impact of contamination on light guiding, a new dry transfer method using a two-layer-composite-structure of polyethylene terephthalate and silica gel was applied to transfer the $PtSe_2$ film with a size of 3 mm × 3 mm from the sapphire substrate to the PDMS sheet [40]. With this method, the transferred 2D material possesses a cleaner and more continuous surface, a lower doping level, and a higher optical transmittance and conductivity than that transferred by thermal release tape and polymethylmethacrylate (PMMA). Therefore, there is little effect of contaminants on the experiment, and the reproducibility of the experiment is satisfactory. Then, the microfiber is sandwiched between a low-refractive-index substrate MgF_2 (with a refractive index of 1.37 at a wavelength of 1.55 μm) and the $PtSe_2$ film supported by PDMS (with a refractive index of 1.413 at a wavelength of 1.55 μm). The microfiber is drawn from single-mode fiber (SMF) using the flame-brushing technique, with a waist diameter of ~7.5 μm, a stretching length of 20 mm, and an insertion loss of 0.1 dB. The total length of the $PtSe_2$ film on the microfiber is about 3 mm, as shown in Fig. 2(b).

Since the microfiber-based SA is used to interact with the evanescent field of light waves through the side of the micro-nanofibers, the $PtSe_2$-based SA has different absorption effects for light with different polarization states in the fiber. In the experiment, we measured the saturable absorption characteristics of the transverse-electric (TE) and transverse-magnetic (TM) modes of the SA by adjusting the polarization controller in the optical path. The polarization-dependent saturable absorption, as shown in Figs. 2(c) and 2(d), is measured by a homemade mode-locked laser with 380 fs wide pulses at 1.55 μm. We found that the absorption of the TE mode is significantly less than that of the TM mode at the same pump power. This is due to the fact that the direction of the electric field of the TE mode is parallel to the plane of the $PtSe_2$, so that the TE mode electromagnetic wave has less interactions with the $PtSe_2$ plane when passing through the device, which results in less propagation loss. The transmittance of the TE mode increased from 24.90% to 29.80%, with a modulation depth of 4.90%, and the saturable intensity is 0.34 GW/cm^2, as shown in Fig. 2(c). The modulation depth of the TM mode is 1.11%, and the saturable intensity is 1.23 GW/cm^2, which are shown in Fig. 2(d). In Table 1, we quantitatively compare our $PtSe_2$-based SA with several nanomaterial-based SAs working around 1.5 μm. It can be seen that the modulation depth of the $PtSe_2$-based SA is comparable to reports of other nanomaterials, while the saturable intensity is larger than those of others. The difference in saturable intensity is mainly due to the structure that we used to fabricate the $PtSe_2$-based SA. With the $PtSe_2$-covered-microfiber structure, the $PtSe_2$ interacted with the evanescent field of the light wave, which is much weaker than the field in the fiber center. Therefore, the saturable intensity of our SA is larger than that of other

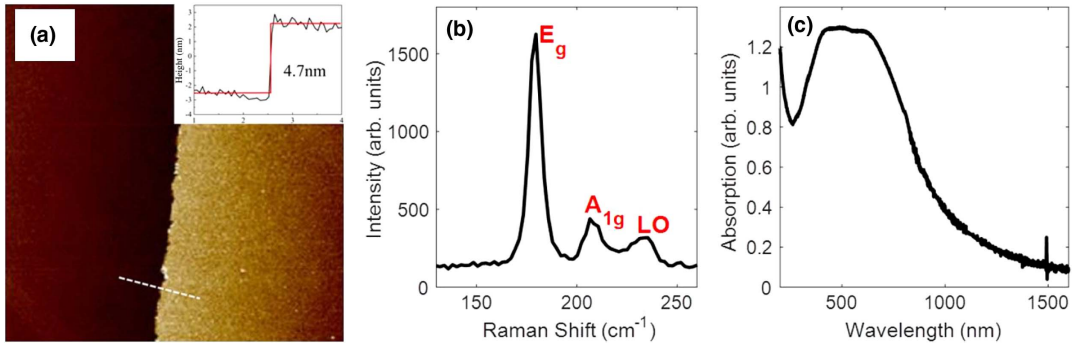

Fig. 1. (a) AFM image of the CVD-grown $PtSe_2$ film on the sapphire substrate. The red curve shows the thickness along the white dashed line. (b) Representative Raman spectrum of $PtSe_2$ film taken at a 514 nm excitation wavelength. (c) Absorption spectrum of the $PtSe_2$ film.

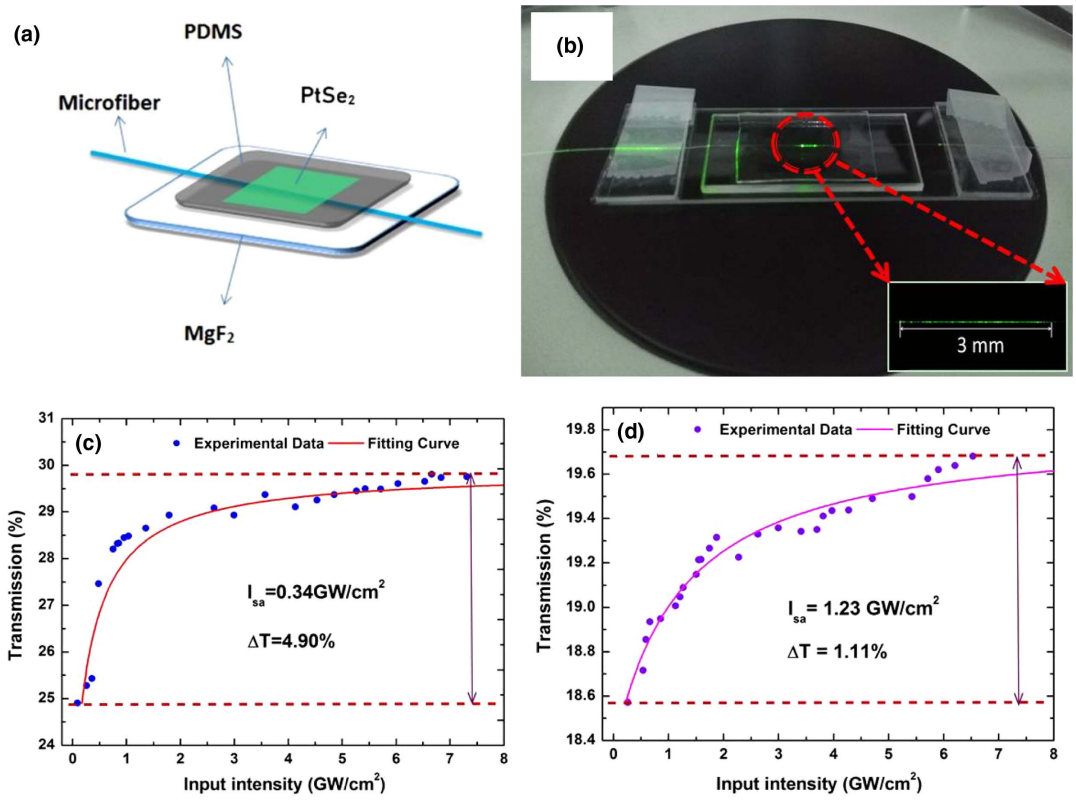

Fig. 2. (a) Structure of the $PtSe_2$-based SA. (b) Optical image and optical microscope image (inset) of the $PtSe_2$-based SA. (c) Nonlinear optical transmission of TE mode in $PtSe_2$-based SA. (d) Nonlinear optical transmission of TM mode in the $PtSe_2$-based SA.

reported results, but the saturable intensity is easily decreased by using a thinner microfiber, which shows the flexibility of the microfiber-based structure.

Using the $PtSe_2$ SA, we built an all-fiber erbium-doped ring laser, as shown in Fig. 3. We used a high-concentration erbium-doped fiber (Thorlabs Er80/4-125) with a length of 95 cm as the gain medium and a laser with a wavelength of 980 nm as a pump source directly through a wavelength-division multiplexer. In addition, there are a polarization controller (PC), a 10:90 output coupler, and a polarization-independent isolator in the cavity. All the optical components, except the erbium-doped fiber, are made of single-mode fibers. The total length of the cavity is 8.7 m. The laser output pulse is detected by a 200 MHz photodetector and a 2 GHz oscilloscope, while the spectrum is monitored by a spectrometer with a resolution of 0.1 nm. The dispersion coefficient of the single-mode fiber is −17 ps/(nm · km), and the dispersion coefficient of the Er-doped fiber is 28 ps/(nm · km). According to the length of the fiber in each part of the resonant cavity, the net cavity dispersion is calculated to be −0.138 ps^2.

3. EXPERIMENTAL RESULTS AND DISCUSSION

In the experiment, when the pump power increases to 65 mW, the laser starts to output stable *Q*-switched pulses. Typical

Table 1. Saturable Absorption Properties for Different Nanomaterial-Based SAs at 1.5 μm and Mode-Locked Lasing Output Properties Based on Them

Material	Modulation Depth	Saturable Intensity	Pulse Duration	Refs.
Single-walled carbon nanotubes	11.20%	15.5 MW/cm^2	0.47 ps	[8]
Graphene	18.17%–65.88%	0.53–1.09 MW/cm^2	1.23 ps	[10]
Graphene oxide	2.6%	60 MW/cm^2	0.20 ps	[13]
BP	8.1%	6.55 MW/cm^2	0.95 ps	[17]
BPQDs	36%	3.3 GW/cm^2	1.08 ps	[18]
Bi_2Te_3	1.7%	630 MW/cm^2	2.94 ps	[19]
Bi_2Te_3	6.20%	28 MW/cm^2	0.32 ps	[22]
MoS_2	4.3%	34 MW/cm^2	0.71 ps	[23]
WS_2	15.1%	157.6 MW/cm^2	1.49 ps	[25]
TiS_2	18%	9.91 MW/cm^2	1.04 ps	[26]
$MoTe_2$	25.50%	9.6 MW/cm^2	0.23 ps	[27]
$PtSe_2$	1.11%–4.90%	0.34–1.23 GW/cm^2	1.02 ps	This work

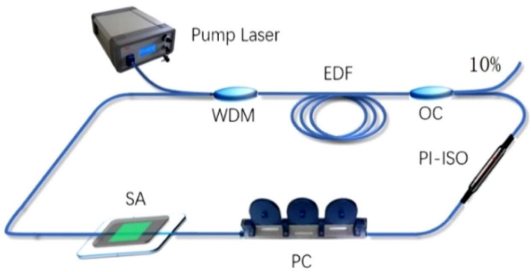

Fig. 3. Structure of the $PtSe_2$-SA-based EDFL. WDM, wavelength division multiplexer; EDF, Er-doped fiber; OC, optical coupler; PI-ISO, polarization-independent isolator; PC, polarization controller; SA, saturable absorber.

Q-switched laser output properties under a pump power of 445 mW are shown in Fig. 4. The repetition rate of a *Q*-switched pulse train is about 79.2 kHz, while the pulse shape is similar to a Gaussian shape with a pulse width of 0.9 μs. The corresponding spectrum is shown in Fig. 4(c), from which we can see that the 3 dB spectral bandwidth of the *Q*-switched output is 1.85 nm and the center wavelength is 1560 nm.

Furthermore, the variations of the *Q*-switched pulse properties with the pump power are also studied. Figure 5(a) shows the repetition rate and the pulse duration as a function of pump power. By increasing the pump power from 92.8 to 445 mW, the repetition rate increases monotonically from 20.5 to 79.2 kHz, and the pulse duration decreases from 4.6 to 0.9 μs, which results from the increase of the pump rate for the upper laser level. The increase of the repetition rate and the reduction of the pulse width present typical features of passively *Q*-switched lasers. The output power increases from 0.91 to 11.34 mW when the pump power varies from 92.8 to 445 mW, and the highest single pulse energy is about 143.2 nJ as presented in Fig. 5(b). This suggests that $PtSe_2$ as an SA can make the laser operate in a stable *Q*-switched state.

Due to the polarization-dependent characteristics of SA, the above-mentioned laser can be switched from a *Q*-switched state to a mode-locked state by adjusting the polarization state. Mode-locked pulses are generated when the pump power increases to about 80 mW. The stable mode-locked state maintains at even pump power up to a maximum of 450 mW, and the output single pulse energy can be up to 0.53 nJ. Figure 6 shows typical output characteristics of the mode-locked laser with a pump power of 250 mW. As presented in Fig. 6(a), the pulse repetition rate is about 23.3 MHz, which matches the cavity length well and indicates that the laser is working in the mode-locked state. Figure 6(b) is the pulse autocorrelation trace that can be well fitted by the hyperbolic secant function with a width of 1.58 ps, which indicates the real pulse width of approximately 1.02 ps. Figure 6(c) is the corresponding optical spectrum, whose 3 dB bandwidth is ~6 nm, and the center wavelength is 1563 nm. There are four groups of sidebands on both sides of the center wavelength, which shows a clear characteristic of the traditional negative dispersion soliton and is consistent with our calculation of the net dispersion in the resonant cavity. The radio-frequency (RF) spectrum of the mode-locking state is measured and shown in Fig. 6(d) with a resolution bandwidth of 300 kHz. The signal-to-noise

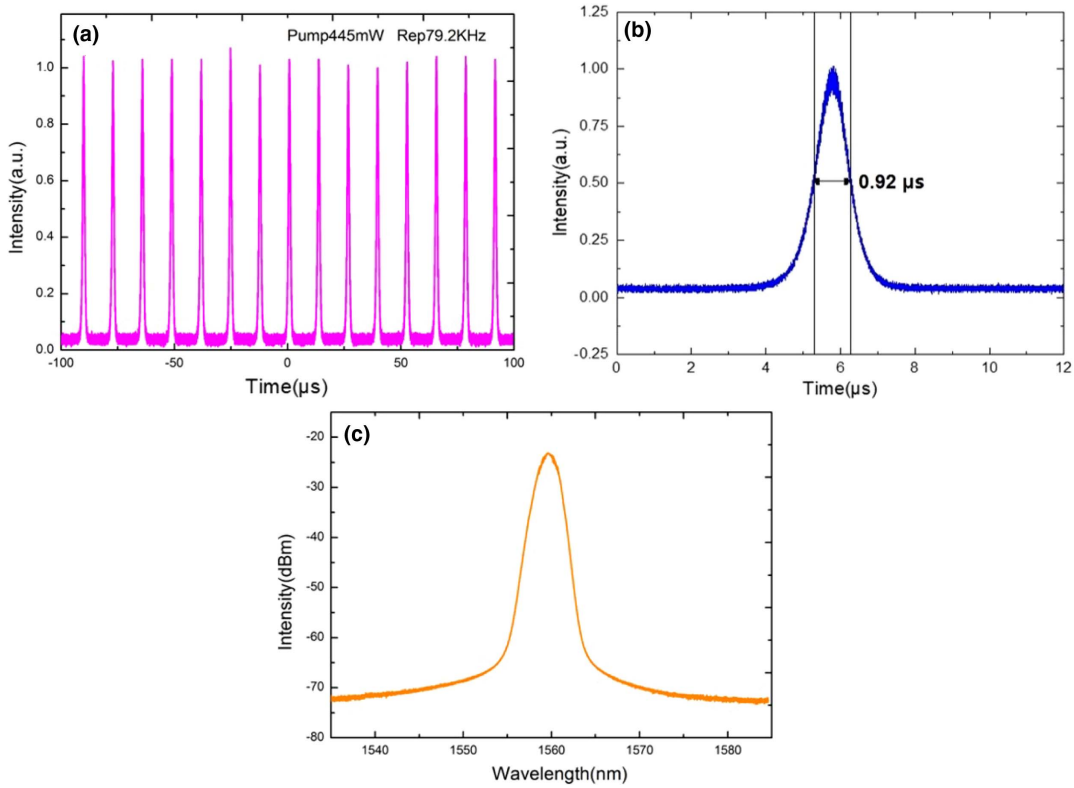

Fig. 4. (a) Output pulse train, (b) single pulse profile, and (c) optical spectrum of the *Q*-switching EDFL at a pump power of 445 mW.

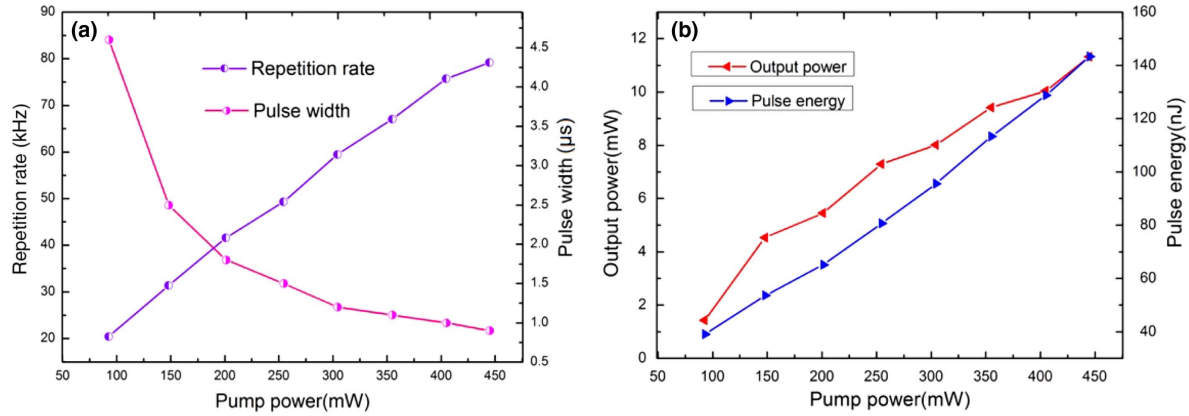

Fig. 5. (a) Pulse repetition rate and pulse width versus pump power. (b) Average output power and single pulse energy vary with pump power.

ratio (SNR), which is up to 61 dB, shows that the fiber laser operates in a highly stable regime. To confirm the long-term stability of the mode-locked operation, fluctuation of the 3 dB spectral bandwidth is measured and shown in the inset of Fig. 6(c). The results show that the mode-locked pulses can be stable for hours. The durations of the mode-locked laser pulses are comparable to those of the reported lasers mode-locked with other nanomaterials as shown in Table 1, which indicates that $PtSe_2$ is a strong competitor for acting as an SA. To confirm the contribution of the $PtSe_2$-based SA to mode-locking operation, we remove the $PtSe_2$ film covering the microfiber and just cover the microfiber with a piece of PDSM, which is the same as the one supporting the $PtSe_2$ film. By carefully adjusting the PC and pump power, no laser pulses can be observed in this case. Therefore, the mode-locking operation is caused by the $PtSe_2$-based SA. Owing to the $PtSe_2$-covered-microfiber structure, $PtSe_2$ interacts with the evanescent field of light waves outside the microfibers. Therefore, this $PtSe_2$-based SA has relatively high damage threshold. Also, the $PtSe_2$ was not damaged during our experiment.

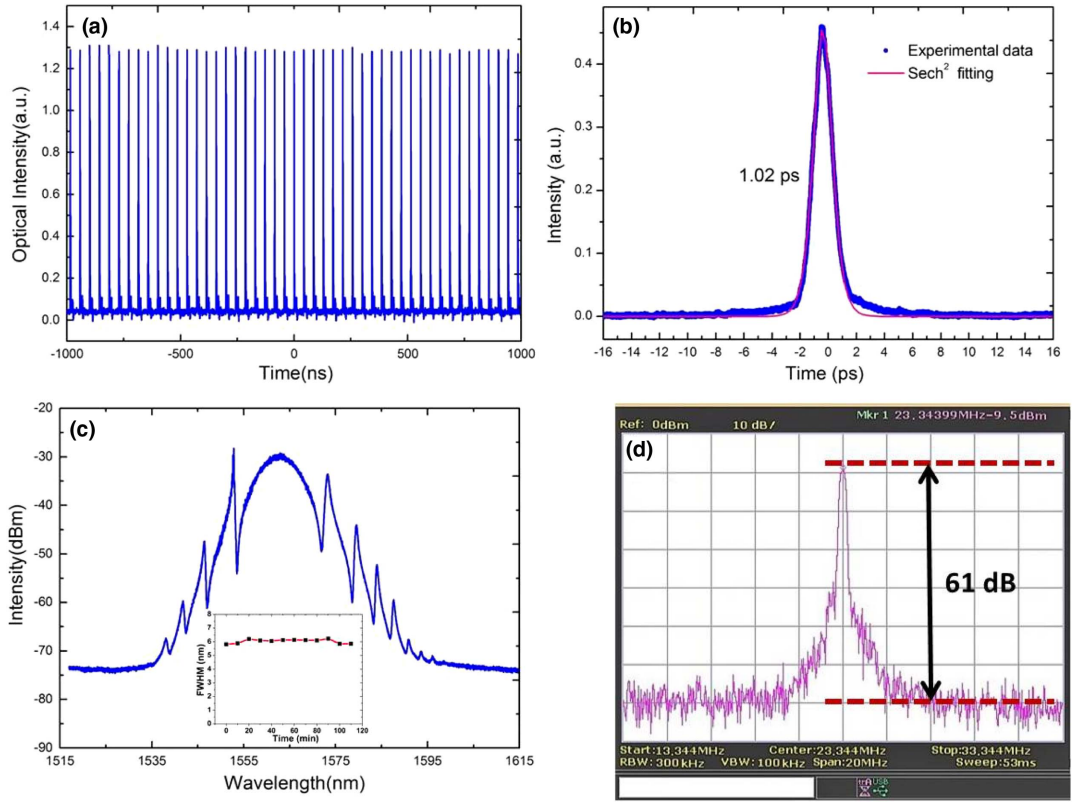

Fig. 6. (a) Output pulse train, (b) the measured autocorrelation trace and its fitted curve, (c) optical spectrum (inset, long-term 3 dB spectral bandwidth fluctuation of the laser), and (d) RF spectrum of the mode-locked EDFL.

4. CONCLUSIONS

In this paper, stable Q-switched and mode-locked EDFLs are obtained by using 4.7 nm thick $PtSe_2$ film as an SA. Self-started Q-switched pulses at 1560 nm were achieved with a threshold pump power of 65 mW. The output power increased from 0.91 to 11.34 mW when pump power increased from 92.8 to 445 mW. The maximum single Q-switched pulse energy is up to 143.2 nJ. A mode-locked EDFL was also obtained for a threshold pump power of 93 mW, with a pulse width of approximately 1.02 ps and maximum single pulse energy of about 0.53 nJ. The results experimentally verify the feasibility of using $PtSe_2$ as an SA. We believe that better performance could be obtained for $PtSe_2$-based mode-locking by optimizing the CVD-grown layer thickness and quality.

Funding. National Natural Science Foundation of China (NSFC) (11174159, 11304166, 61405139, 61475076); Natural Science Foundation of Tianjin City (14JCYBJC16400); International Cooperation Program sponsored by Ministry of Education of the People's Republic of China (MOE); Chinese National Key Basic Research Special Fund (2011CB922003); National Science Fund for Talent Training in Basic Sciences (J1103208).

REFERENCES

1. R. Paschotta, R. Häring, E. Gini, H. Melchior, and U. Kelle, "Passively Q-switched 0.1-mJ fiber laser system at 1.53 mm," Opt. Lett. **24**, 388–390 (1999).
2. Y. Wang and C. Q. Xu, "Actively Q-switched fiber lasers: switching dynamics and nonlinear processes," Prog. Quantum Electron. **31**, 131–216 (2007).
3. C. Wu and N. K. Dutta, "High-repetition-rate optical pulse generation using a rational harmonic mode-locked fiber laser," IEEE J. Quantum Electron. **36**, 721–727 (2000).
4. H. Zhang, D. Y. Tang, L. M. Zhao, Q. L. Bao, and K. P. Loh, "Large energy mode locking of an erbium-doped fiber laser with atomic layer grapheme," Opt. Express **17**, 17630–17635 (2009).
5. Z. Kang, X. Guo, Z. Jia, Y. Xu, L. Liu, D. Zhao, G. Qin, and W. Qin, "Gold nanorods as saturable absorbers for all-fiber passively Q-switched erbium-doped fiber laser," Opt. Mater. Express **3**, 1986–1991 (2013).
6. H. Guo, M. Feng, F. Song, H. Li, A. Ren, X. Wei, Y. Li, X. Xu, and J. Tian, "Q-switched erbium-doped fiber laser based on silver nanoparticles as a saturable absorber," IEEE Photon. Technol. Lett. **28**, 135–138 (2016).
7. Z. Wang, L. Zhan, M. Qin, J. Wu, L. Zhang, Z. Zou, and K. Qian, "Passively Q-switched Er-doped fiber lasers using alcohol," J. Lightwave Technol. **33**, 4857–4861 (2015).
8. D. D. Han, X. M. Liu, Y. D. Cui, G. X. Wang, C. Zeng, and L. Yun, "Simultaneous picosecond and femtosecond solitons delivered from a nanotube-mode-locked all-fiber laser," Opt. Lett. **39**, 1565–1568 (2014).
9. X. H. Li, Y. G. Wang, Y. S. Wang, W. Zhao, X. C. Yu, Z. P. Sun, X. P. Cheng, X. Yu, Y. Zhang, and Q. J. Wang, "Nonlinear absorption of SWNT film and its effects to the operation state of pulsed fiber laser," Opt. Express **22**, 17227–17235 (2014).
10. Q. Bao, H. Zhang, Z. Ni, Y. Wang, L. Polavarapu, Z. Shen, Q.-H. Xu, D. Tang, and K. P. Loh, "Monolayer graphene as a saturable absorber in a mode-locked laser," Nano Res. **4**, 297–307 (2011).
11. Y. F. Song, L. Li, H. Zhang, D. Y. Shen, D. Y. Tang, and K. P. Loh, "Vector multi-soliton operation and interaction in a graphene mode-locked fiber laser," Opt. Express **21**, 10010–10018 (2013).
12. Q. Sheng, M. Feng, W. Xin, T. Han, Y. Liu, Z. Liu, and J. Tian, "Actively manipulation of operation states in passively pulsed fiber lasers by using graphene saturable absorber on microfiber," Opt. Express **21**, 14859–14866 (2013).
13. J. Xu, J. Liu, S. Wu, Q.-H. Yang, and P. Wang, "Graphene oxide mode-locked femtosecond erbium-doped fiber lasers," Opt. Express **20**, 15474–15480 (2012).
14. J.-H. Cai, H. Chen, S.-P. Chen, and J. Hou, "Compressibility of dissipative solitons in mode-locked all-normal-dispersion fiber lasers," J. Lightwave Technol. **36**, 2142–2151 (2018).
15. Y. H. Lin, Y. C. Chi, and G. R. Lin, "Nanoscale charcoal powder induced saturable absorption and mode-locking of a low-gain erbium-doped fiber-ring laser," Laser Phys. Lett. **10**, 055105 (2013).
16. S. H. Lee and H. S. Suh, "Near infrared standard sources, generated by electro-optic frequency comb, using injection-locked DFB laser," Opt. Commun. **312**, 7–10 (2014).
17. Y. Chen, G. Jiang, S. Chen, Z. Guo, X. Yu, C. Zhao, H. Zhang, Q. Bao, S. Wen, D. Tang, and D. Fan, "Mechanically exfoliated black phosphorus as a new saturable absorber for both Q-switching and mode-locking laser operation," Opt. Express **23**, 12823–12833 (2015).
18. Y. Xu, Z. Wang, Z. Guo, H. Huang, Q. Xiao, H. Zhang, and X.-F. Yu, "Solvothermal synthesis and ultrafast photonics of black phosphorus quantum dots," Adv. Opt. Mater. **4**, 1223–1229 (2016).
19. Z. Luo, M. Liu, H. Liu, X. Zheng, A. Luo, C. Zhao, H. Zhang, S. C. Wen, and W. Xu, "2 GHz passively harmonic mode-locked fiber laser by a microfiber-based topological insulator saturable absorber," Opt. Lett. **38**, 5212–5215 (2013).
20. Z. Luo, Y. Huang, J. Weng, H. Cheng, Z. Lin, B. Xu, Z. Cai, and H. Xu, "1.06 μm Q-switched ytterbium-doped fiber laser using few-layer topological insulator Bi_2Se_3 as a saturable absorber," Opt. Express **21**, 29516–29522 (2013).
21. J. F. Li, H. Y. Luo, L. L. Wang, C. J. Zhao, H. Zhang, H. P. Li, and Y. Liu, "3-μm mid-infrared pulse generation using topological insulator as the saturable absorber," Opt. Lett. **40**, 3659–3662 (2015).
22. P. Yan, R. Lin, S. Ruan, A. Liu, and H. Chen, "A 2.95 GHz, femtosecond passive harmonic mode-locked fiber laser based on evanescent field interaction with topological insulator film," Opt. Express **23**, 154–164 (2015).
23. H. Liu, A. Luo, F. Wang, R. Tang, M. Liu, Z. Luo, W. Xu, C. Zhao, and H. Zhang, "Femtosecond pulse erbium-doped fiber laser by a few-layer MoS_2 saturable absorber," Opt. Express **39**, 4591–4594 (2014).
24. P. G. Yan, A. J. Liu, Y. S. Chen, H. Chen, S. C. Ruan, C. Y. Guo, S. F. Chen, I. L. Li, H. P. Yang, J. G. Hu, and G. Z. Cao, "Microfiber-based WS_2-film saturable absorber for ultra-fast photonics," Opt. Mater. Express **5**, 479–489 (2015).
25. P. G. Yan, H. Chen, J. D. Yin, Z. H. Xu, J. R. Li, Z. K. Jiang, W. F. Zhang, J. Z. Wang, I. L. Li, Z. P. Sun, and S. C. Ruan, "Large-area tungsten disulfide for ultrafast photonics," Nanoscale **9**, 1871–1877 (2017).
26. Y. Q. Ge, Z. F. Zhu, Y. H. Xu, Y. X. Chen, S. Chen, Z. M. Liang, Y. F. Song, Y. S. Zou, H. B. Zeng, S. X. Xu, H. Zhang, and D. Y. Fan, "Broadband nonlinear photoresponse of 2D TiS_2 for ultrashort pulse generation and all-optical thresholding devices," Adv. Opt. Mater. **6**, 1701166 (2018).
27. J. T. Wang, Z. K. Jiang, H. Chen, J. R. Li, J. D. Yin, J. Z. Wang, T. C. He, P. G. Yan, and S. C. Ruan, "High energy soliton pulse generation by a magnetron-sputtering-deposition-grown $MoTe_2$ saturable absorber," Photon. Res. **6**, 535–541 (2018).
28. J. T. Wang, H. Chen, Z. K. Jiang, J. D. Yin, J. Z. Wang, M. Zhang, T. C. He, J. Z. Li, P. G. Yan, and S. C. Ruan, "Mode-locked thulium-doped fiber laser with chemical vapor deposited molybdenum ditelluride," Opt. Lett. **43**, 1998–2001 (2018).
29. K. F. Mak, C. Lee, J. Hone, J. Shan, and T. F. Heinz, "Atomically thin MoS_2: a new direct-gap semiconductor," Phys. Rev. Lett. **105**, 136805 (2010).
30. A. Ciarrocchi, A. Avsar, D. Ovchinnikov, and A. Kis, "Thickness-modulated metal-to-semiconductor transformation in a transition metal dichalcogenide," Nat. Commun. **9**, 919 (2018).
31. Y. L. Wang, L. F. Li, W. Yao, S. Song, J. T. Sun, J. Pan, X. Ren, C. Li, E. Okunishi, Y. Wang, E. Wang, Y. Shao, Y. Y. Zhang, H. Yang, E. F. Schwier, H. Iwasawa, K. Shimada, M. Taniguchi, Z. Cheng, S. Zhou, S. Du, S. J. Pennycook, S. T. Pantelides, and H. Gao, "Monolayer $PtSe_2$, a new semiconducting transition-metal-dichalcogenide, epitaxially grown by direct selenization of Pt," Nano Lett. **15**, 4013–4018 (2015).

32. Y. Zhao, J. Qiao, Z. Yu, P. Yu, K. Xu, S. P. Lau, W. Zhou, Z. Liu, X. Wang, W. Ji, and Y. Chai, "High-electron-mobility and air-stable 2D layered $PtSe_2$ FETs," Adv. Mater. **29**, 1604230 (2017).
33. W. X. Zhang, J. T. Qin, Z. S. Huang, and W. L. Zhang, "The mechanism of layer number and strain dependent bandgap of 2D crystal $PtSe_2$," J. Appl. Phys. **122**, 205701 (2017).
34. S. Sattar and U. Schwingenschlögl, "Electronic properties of graphene–$PtSe_2$ contacts," ACS Appl. Mater. Interfaces **9**, 15809–15813 (2017).
35. P. F. Li, L. Li, and X. C. Zeng, "Tuning the electronic properties of monolayer and bilayer $PtSe_2$ via strain engineering," J. Mater. Chem. C **4**, 3106–3112 (2016).
36. L. Li, M. Engel, D. B. Farmer, S. Han, and H.-S. P. Wong, "High-performance p-type black phosphorus transistor with scandium contact," ACS Nano **10**, 4672–4677 (2016).
37. Z. Huang, W. Zhang, and W. Zhang, "Computational search for two-dimensional MX2 semiconductors with possible high electron mobility at room temperature," Materials **9**, 716–729 (2016).
38. W. X. Zhang, Z. S. Huang, W. L. Zhang, and Y. Li, "Two-dimensional semiconductors with possible high room temperature mobility," Nano Res. **7**, 1731–1737 (2014).
39. M. O'Brien, N. McEvoy, C. Motta, J.-Y. Zheng, N. C. Berner, J. Kotakoski, K. Elibol, T. J. Pennycook, J. C. Meyer, C. Yim, M. Abid, T. Hallam, J. F. Donegan, S. Sanvito, and G. S. Duesberg, "Raman characterization of platinum diselenide thin films," 2D Mater. **3**, 021004 (2016).
40. X. D. Chen, Z. B. Liu, C. Y. Zheng, F. Xing, X. Q. Yan, Y. S. Chen, and J. G. Tian, "High-quality and efficient transfer of large-area graphene films onto different substrates," Carbon **56**, 271–278 (2013).